Numerical and experimental analysis of airborne particles control in an operating theater

Francesco Romano [a, *], Luca Marocco [a, 1], Jan Gustén [b, 2], Cesare M. Joppolo [a, 3]

[a] Politecnico di Milano, Dipartimento di Energia, Via Lambruschini 4, 20156, Milan, Italy
[b] Chalmers University of Technology, Civil and Environmental Engineering/Building Services Engineering, Maskingränd 2, SE-41296, Gothenburg, Sweden

Received 30 December 2014
Received in revised form
17 February 2015
Accepted 4 March 2015
Available online 12 March 2015

1. Introduction

The design of a ventilation system for an Operating Theater is aimed to prevent the risk of infections during surgical operations, while maintaining an adequate comfort condition for the patient and the surgical staff [1]. Surgical Site Infections (SSI) typically occur on site during an operation [2]. They are found to be associated with increased postoperative length of stay, increased costs, hospital re-admission rates and the use of antimicrobial agents [3]. The interest to intervene in a significant way to reduce the sources of these contingencies is obvious. There are many aspects that could influence these type of infections: factors related to the patient (as the susceptibility to infections), factors related to the surgical site and others related to the ventilation system of the OT environment. The contamination on surgical site is an unavoidable reason for the occurrence of SSIs. Primary sources of contamination in OTs are airborne particles (biologically active or inert) released by the human body during normal activity [4]. Their diameter size varies typically between 0.5 and 10 μm and their settling on the surgical site could be the cause of potential infections [5]. A surgeon during activity may release about 1000 airborne particles/min [1], while the patient is not usually a significant contaminant source because its movements are minimal [6]. Moreover, the beneficial use of surgical face masks has yet to be conclusively demonstrated [7]. The works of Stacey et al. [8], Charneley [9], Whyte et al. [10] and Lidwell et al. [11] have shown the important correlation between the airborne wound contamination and the ventilation system. In particular, they have established a linear relationship between the level of bacterial air contamination and the frequency

* Corresponding author. Tel.: +39 02 2399 3823, +39 333 5239269 (mobile); fax: +39 02 2399 3913.
E-mail addresses: francesco.romano@polimi.it (F. Romano), luca.marocco@polimi.it (L. Marocco), jan.gusten@chalmers.se (J. Gustén), cesare.joppolo@polimi.it (C.M. Joppolo).
[1] Fax: +39 02 2399 3913.
[2] Tel.: +46 (0)31 772 1144, +46 (0)705 3459 96 (mobile); fax: +46 (0)31 772 1152.
[3] Tel.: +39 02 2399 3856, +39 320 8393654 (mobile); fax: +39 02 2399 3913.

of ”deep sepsis” following surgery operations. Therefore, a proper ventilation system is crucial in OT environments. These can be considered as special cleanrooms where different types of processes (operations) are carried out by different personnel (medical staff). As a consequence, many national and European standards, which deal with operating theaters and related controlled environments, have common roots with the standards and procedures used in cleanrooms, as the ISO 14644-1 [12] for airborne particle contamination and the ISO 14698 [13] for microbiological contamination. In the last years many national standards and technical reports have been issued with the aim to rule the design and the performance test procedures of operating theaters from the point of view of airborne contamination control. However, there is no complete consensus and uniformity among the various standards. The performance tests for airborne particle contamination in OTs are quite time consuming and expensive. Moreover, availability, reliability and cleanliness are important parameters for OTs, especially in emergency cases. Therefore the time available for carrying out real contamination and ventilation performance tests is always short and, as often occurs, practically null. The advantages of using CFD are many. It is cheaper and less invasive than the traditional experimental test campaign and it allows to investigate different solutions and case scenarios without interfering with the normal operation of an OT. Therefore, it may be a useful tool for the design, testing and the comparison of ventilation performances of existing OTs or new ventilation alternatives [14]. Several CFD studies of indoor ventilation systems have been already carried out. Swift et al. [15] have discussed the impact of different air distribution strategies on infection control and the effects of lightings and obstructions on unidirectional air flow systems. Numerical simulations on a vertical and a horizontal laminar airflow distribution in OT have investigated their impact on the bacteria-carrying particle distribution, even though a complete experimental validation has not been carried out [2]. Memarzadeh and Manning [16] have used CFD to show that, when the design is appropriate, unidirectional flow conditions are the best choice for controlling the risk of contaminant deposition in a surgical operating room. Memarzadeh and Jiang [17] have numerically investigated the impact of the ceiling height on the level of contaminants present at the surgical site in an operating theater. Kameel et al. [18] have numerically evaluated the airflow regimes, relative humidity and heat transfer characteristics under actual OT's geometrical and operating conditions. Brohus et al. [19] have investigated the influence of two disturbances in an operating room: the door opening during an operation and the activity level of the staff. The same study has also been carried out by Shuyun et al. [20], and Tung et al. [21] for the specific application in local operating theaters.

The accuracy of OT's CFD simulations strongly depends on the considered obstacles in the domain, e.g. human occupants and medical equipment, as well as on the appropriate settings of boundary conditions and numerical simulation parameters, such as contaminant sources and heat fluxes, as demonstrated by Srebric et al. [22] and [3]. All these previous works have been validated through comparison with experimental data, even though they have only treated downward laminar (unidirectional) airflow with HEPA (High Efficiency Particulate Air Filter) filtered air at uniform velocity. On the contrary only few works have dealt with the application of CFD simulations to national standard performance tests on air contamination control [23–27]. Traversari et al. [28] have evaluated the airborne bacterial contamination in an OT by comparing two air diffusion systems, i.e. a unidirectional horizontal flow (UDHF), and a unidirectional downward flow (UDDF), partly using the procedure described in standard DIN 1946-4 [27].

The present research work is aimed to numerically and experimentally evaluate the airflow, temperature and airborne particles distribution of an OT in “operational conditions” with a layout according to the German standard DIN 1946-4 [27]. Moreover the effectiveness of a differential air diffusion system in reducing the particle concentration in the surgical zone close to the operating table is investigated. The supply air comes from a ceiling filter system composed of 23 H14 filtering units, which assures an unidirectional flow on the surgical table and close to the staff area. The configuration of the operating theater and the procedures for the experimental test of the protection grade SG are chosen in accordance with the German standard DIN 1946-4 [27], while the ISO 14644-1 [12] are used for the ISO N class evaluation. The aim of the protection grade SG is a quantitative evaluation of the level of protection provided by an OT ventilation system against the entry of external and internal particle contamination loads into the protected area, taking into consideration airflow pattern obstacles and heat loads. The German standard DIN 1946-4 [27] has been chosen because it presents a complete and appropriate test procedure for evaluating the performance of a ventilation system in an operating theater with respect to airborne particle control at operational state (simulated conditions).

2. Case study

The plan dimensions of the operating theater used as case study are of 7 m, with a net height of 3 m. The theater is provided with a unidirectional ceiling diffuser composed of 23 terminal HEPA H14 filters (each with a net area of 0.521 m $\times$ 0.521 m) installed in a plenum of 3 m $\times$ 3 m. The main characteristic of this ceiling filter system is the differentiation of the supply air velocity. Indeed, as shown in Fig. 1, the three central terminal filters, located above the operating table (Fig. 2) and labeled High Speed (HS) filters, release air at a velocity of 0.45 m/s, while the six Medium Speed (MS) filters around them release air at a velocity of 0.35 m/s. The periphery of the ceiling diffuser is equipped with H14 filters with a low air speed value (LS) equal to 0.25 m/s.

At each corner of the OT, two extraction grilles are installed, as shown in Fig. 1. Two led-based scialitic lamps are positioned in the ceiling, facing the operating table in the middle of the OT (see Fig. 1). The ventilation system of the OT is designed to ensure an ISO 5 class in ‘operation occupational state’, conforming to the ISO 14644-1 [12]. In order to respect the limitations in terms of air quality and contamination control, 6791 m^3/h (or 45 Air Changes per Hour - ACH) of air is injected from the ceiling filters. Of these, 2500 m^3/h (or 17 ACH) is fresh air while the rest of the airflow rate was recirculated. In order to avoid the risk of contaminant infiltrations from adjacent environments (e.g. ancillary rooms and corridors), an overpressure of 15 Pa is maintained in the OT by extracting 6600 m^3/h of air (or 47 ACH), while 191 m^3/h flows out through the main and service doors, that have a permanent open slit of 5 mm along the side close to the floor. The supply air at the ceiling filters has a design temperature of 20 °C and 50% relative humidity.

3. Computational model

Steady state numerical simulations have been carried out using Ansys© FLUENT 14.5.7. The 3D computational domain of the OT case study has been discretized with an unstructured mesh, made of tetrahedral elements. A grid independence study has been carried out with two different grid sizes, resulting in 5.5 $\times$ 10^6 and 10 $\times$ 10^6 cells. The mesh refinements have been applied in the regions with the highest gradients of transported quantities, i.e. air inlet, air outlet, and especially below the ceiling diffuser, in order to capture the main flow and heat transfer features. No differences in the results could be appreciated between the two meshes. The non-

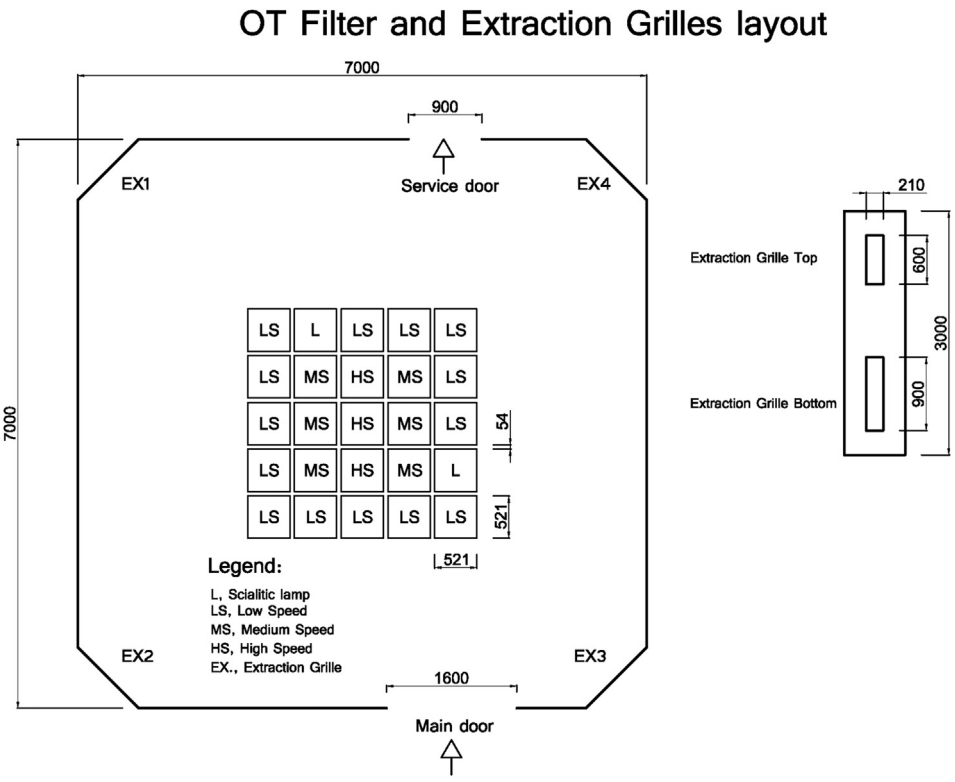

Fig. 1. OT Isometric view of case study and H14 filters distribution in the ceiling filter.

dimensional distance of the near-wall cells has been kept in the range $1 \leq y^{+} \leq 7$ for the entire computational domain in the inner, central and outer zone of the OT, respectively. An average cell size of 0.035, 0.05 and 0.08 m has been used.

As shown by Zhang and Chen [29] both the Eulerian–Eulerian and the Eulerian-Lagrangian methods can well predict the steady-state particle concentration distribution. In this work an Eulerian-Lagrangian model (so called Discrete Phase Model-DPM) has been used, where the continuous gas phase (air) has been modeled with an Eulerian approach, while the solid dispersed phase (airborne particles) with a Lagrangian approach. Therefore, the fluid phase has been treated as a continuum by solving the Navier–Stokes equations, while the dispersed phase has been solved by tracking a large number of particles through the calculated flow field. For a steady flow of constant thermo-physical properties and with negligible buoyancy and viscous dissipation effects, the time-averaged governing equations for momentum and energy can be written as:

$$\overrightarrow{u} \cdot \nabla \overrightarrow{u} = -\frac{1}{\rho} \cdot \nabla P + (\nu + \nu_t) \cdot \nabla^2 \overrightarrow{u} \tag{1}$$

$$\overrightarrow{u} \cdot \nabla T = \left(\frac{\nu}{Pr} + \frac{\nu_t}{Pr_t} \right) \cdot \nabla^2 T \tag{2}$$

In the above Eq. (1) ρ is the air density, P is the mean static pressure, $\overrightarrow{u}$ is the mean velocity vector, ν is the kinematic viscosity and ν_t is the turbulent viscosity. This last has been evaluated using

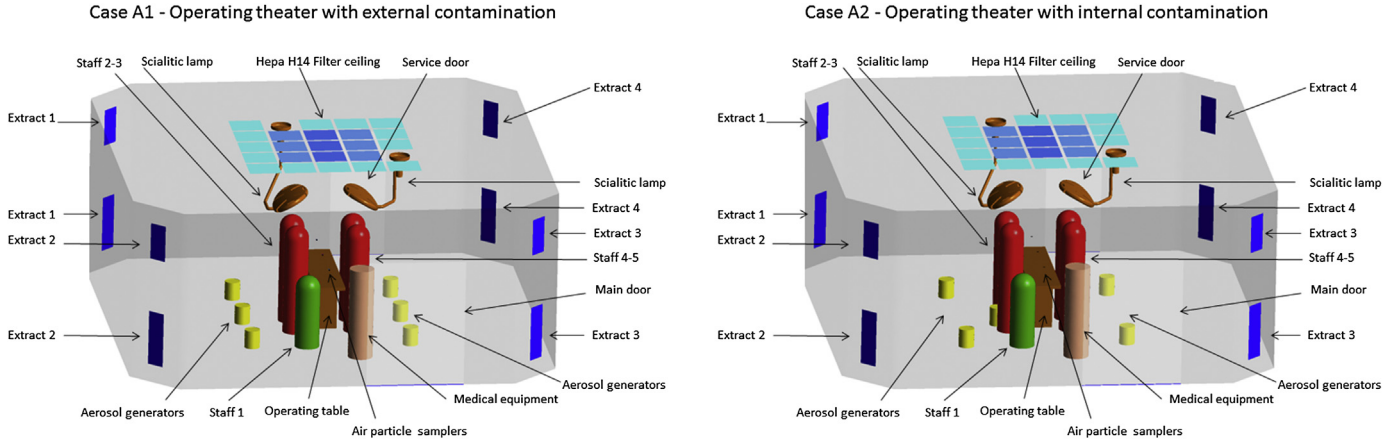

Fig. 2. Operating Theater layouts. Case A1, external contamination layout; Case A2, internal contamination layout.

Table 1
Simulation parameters of the operating theater.

Objects	Surface area [m^2]	Heat flux [W/m^2]	Velocity [m/s]	Boundary condition
Staff 2, 3, 4, 5	2.262	44,21		no slip constant heat flux
Staff 1	1.51	66.31	–	no slip constant heat flux
Medical equipment	1.76	170.52	–	no slip constant heat flux
Operating table (upper surface)	1	–	–	no slip adiabatic
Scialitic lamp (lower surface)	0.56 × 2	215.52 × 2	–	no slip constant heat flux
Aerosol generator	0.567 × 6	159 × 6	0.28	constant velocity 5% turbulence intensity particle diameter 0.5 μm
Air inlet - LS filter	0.271 × 14	–	0.25	constant velocity 5% turbulence intensity
Air inlet - MS filter	0.271 × 6	–	0.35	constant velocity 5% turbulence intensity
Air inlet - HS filter	0.271 × 3	–	0.45	constant velocity 5% turbulence intensity
Outlet air- Top extraction	0.126 × 4	–	–	zero gradient
Outlet air- Bottom extraction	0.189 × 4	–	–	zero gradient
OT floor	47.9	–	–	no slip/adiabatic
Particle sampling probe (inlet section)	0.054 × 3	–	–	no slip/adiabatic

the realizable $\kappa-\varepsilon$ turbulence model [30], which has already proven to be appropriate for calculating airflow and heat transfer phenomena in complex ventilated indoor environments [22]. In Eq. (2) T is the mean static temperature, Pr is the Prandtl number, and $Pr_t = 0.85$ is the turbulent Prandtl number.

The trajectory of a discrete phase particle is calculated by integrating the force balance acting on it:

$$\frac{du_p}{dt} = F_D \cdot \left(\vec{u} - \vec{u}_p\right) + g \cdot \rho_p \cdot \left(1 - \frac{\rho}{\rho_p}\right) + O\left(\frac{\rho}{\rho_p}\right) \tag{3}$$

In the above equation the subscript$p$ refers to particles, g is the acceleration of gravity, O is the order of magnitude operator and F_D is defined as follows:

$$F_D = \frac{18 \cdot \mu}{\rho_p \cdot d_p^2} \cdot \frac{C_D \cdot \mathrm{Re}_p}{24} \tag{4}$$

Here Re_p is the particle's Reynolds number defined as:

$$\mathrm{Re}_p = \frac{\left|\vec{u} - \vec{u}_p\right| \cdot d_p}{\nu} \tag{5}$$

The drag coefficient C_D in Eq. (4) has been evaluated through the Morsi and Alexander correlation [31], that adjusts the value of C_D for a spherical particle over a wide range of Re_p:

$$C_D = \frac{\xi_1}{\mathrm{Re}_p} + \frac{\xi_2}{\mathrm{Re}_p^2} + \xi_3 \tag{6}$$

where the coefficients ξ_i are also functions of Re_p.

From Eq. (3) follows that in gas–liquid flows, where the gas-to-particle density ratio is low, the only two contributions to the particle's linear momentum variation are the first two terms, namely the drag and gravity force.

Because of the low volume fraction occupied by the particles (lower than 8%), a one-way coupling between the phases has been considered, i.e. the gas influences the particles via drag and turbulence but the particles have no influence on the gas [32]. Moreover, also the interaction between the particles has been assumed to be negligible. This has been verified during the post-processing of the results, by checking that the following condition was verified [33]:

$$d_p \leq \frac{1.33 \cdot \nu}{Z \cdot \sigma} \tag{7}$$

In the above equation, Z is the ratio between the particles mass flow rate and the gas mass flow rate and σ is the standard deviation of the particles fluctuating velocity, which is of the order of magnitude of the square root of the turbulent kinetic energy, k, [34]. Furthermore, due to the considered particle diameters, the corresponding deposition velocity and loss deposition coefficient were low enough to allow neglecting particle deposition effects [29].

The SIMPLE algorithm has been used for the pressure–velocity coupling. The diffusion terms are discretized with a central-

Table 2
List of the simulated scenarios with a brief description.

Name	Layout type	Lamp frame	Boundary conditions
A1	External contamination	2	2 closed doors with slits opened All extraction grilles available
A2	Internal contamination	2	2 closed doors with slits opened All extraction grilles available
B2	Internal contamination	2	2 closed doors with slits opened Extraction grilles (EX1 top and bottom) closed at corner 1 (see Figs. 2–3)
C2	Internal contamination	2	Sliding door opened, service door closed All extraction grilles available

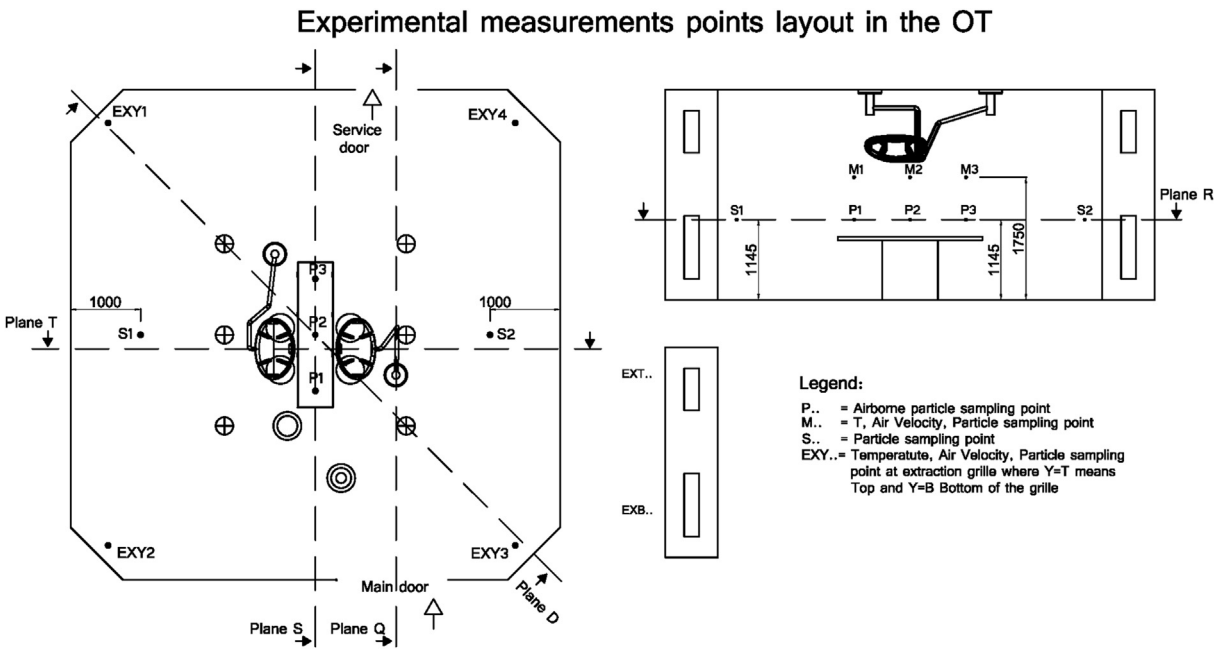

Fig. 3. Experimental measurements points layout for case A1 and A2.

difference scheme while a second-order upwind scheme is used for the convective terms [28]. Adaptive wall-functions, the so called (*enhanced wall treatment* [32]) have been employed. The exposed surfaces of the surgical staff, medical equipment and the downward facing surfaces of the scialitic lamps have been given constant heat flux boundary conditions, while all other surfaces have been considered as adiabatic. No-slip conditions have been enforced at all walls. The air has been injected at constant velocity from the differential diffusion system and from the particle generators. A zero-gradient boundary condition for all transported quantities has been applied at the extraction grilles. The particles have been injected from six aerosol generators close to the operating table and shown in Fig. 2, as suggested by DIN 1946-4 [27]. Their initial velocity value has been set at 0.28 m/s and their direction normal to the generator's surface. The boundary conditions used are summarized in Table 1. A converged solution for the flow has been considered to be reached when all the following conditions were satisfied: a) constant average drag on the walls (b) scaled residuals [32] of continuity, momentum, energy and turbulence parameters below 10^{-6}.

Because of the one-way coupling between the two phases, the particles have been injected only after having solved the airflow field. The particles have been released from the sources at a constant rate in a readily constant airflow. Once all trajectories have been calculated, the particle concentration in each computational cell has been determined as:

$$C_{p,j} = \frac{\sum_{i=1}^{N} \dot{n}_i \cdot \Delta t_{(i,j)}}{V_j} \tag{8}$$

In the above equation the indexes i and j refer to the ith trajectory and jth cell, respectively, while C_p is the mean particle concentration in a cell, V is the volume of a computational cell, $\Delta t_{(i,j)}$ is the time required for a particle to traverse the jth cell on the ith trajectory, i.e. the particle residence time in a cell, and $\dot{n}_i(d_p)$ is the number flow rate associated with diameter size d_p on the ith trajectory:

$$\dot{n}_i(d_p) = \frac{f(d_p) \cdot \dot{m}_i}{\frac{\pi}{6} \cdot \rho_p \cdot d_p^3} \tag{9}$$

where $\dot{m}_i$ is the mass flow associated with the ith trajectory and $f(d_p)$ is the fraction of particle mass associated with size diameter d_p on trajectory i.

As already explained, particle deposition has been neglected. Moreover, in order to determine an upper value for the particle concentration, to all the surfaces, except the outlet grilles, an ideal reflection model has been applied, i.e. the impacting particle is rebounded maintaining the same magnitude and direction for the tangential wall velocity component and same magnitude but opposing direction for the wall normal velocity component. Otherwise, a particle hitting the outlet grilles has been considered

Table 3
Comparison between experimental and simulated data of particle concentration and protection class, SG for scenario A1 and A2 according to DIN 1946-4 [27].

Scenario A1 – External contamination					Scenario A2 – Internal contamination				
Location	Experimental		Numerical		Location	Experimental		Numerical	
	PP/m^3 (≥0.5 μm)	SG	PP/m^3 (≥0.5 μm)	SG		PP/m^3 (≥0.5 μm)	SG	PP/m^3 (≥0.5 μm)	SG
P1	0	5	0	5	P1	0	5	0	5
P2	1438	4.4	0	5	P2	1576	4.4	0	5
P3	0	5	0	5	P3	0	5	0	5

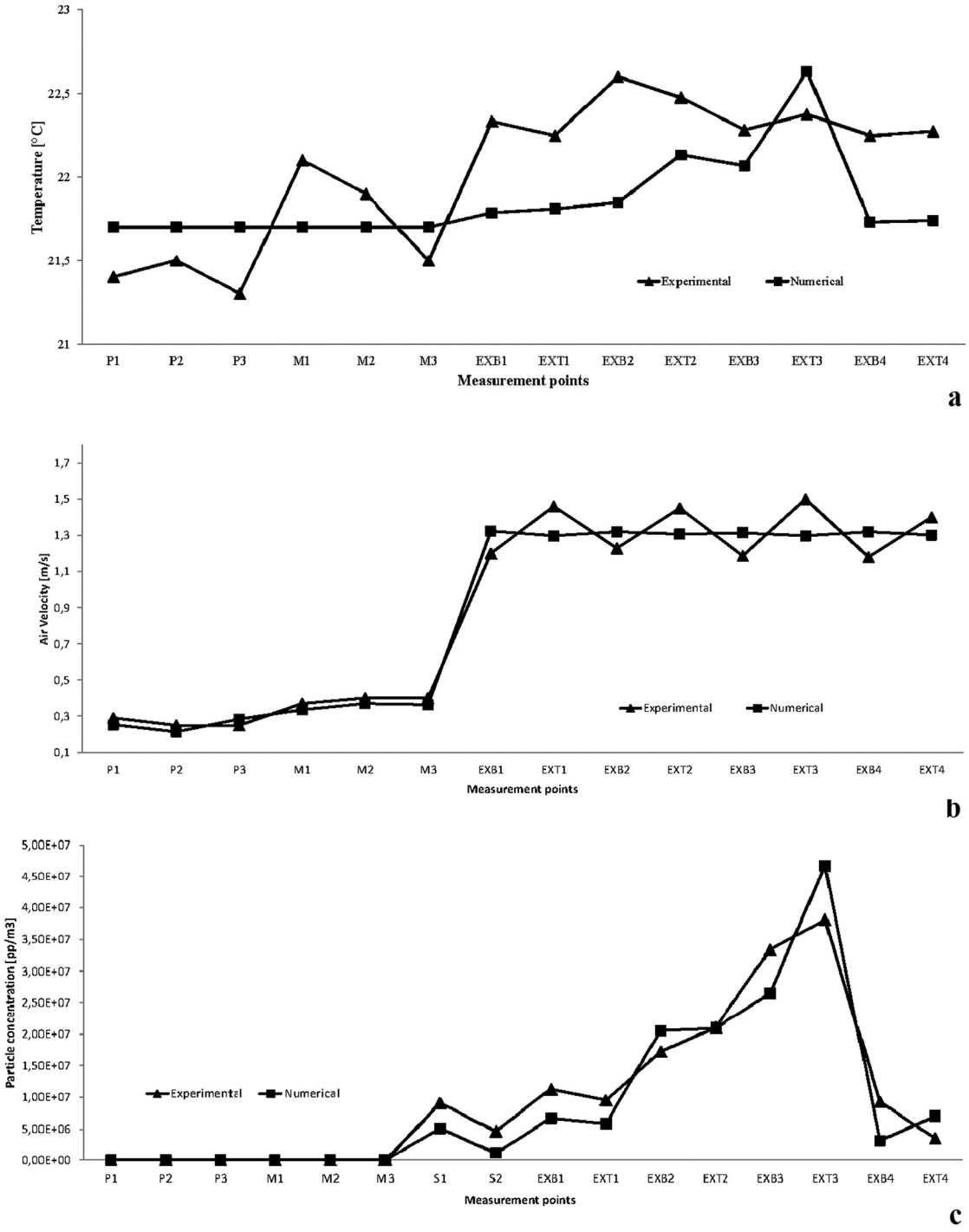

Fig. 4. Comparison of experimental and numerical results. Temperature (a), air velocity (b) and particle concentration (≥0.5 μm) for different locations (c). Average values of cases A1 and A2.

as leaving the domain and thus its trajectory has not been computed anymore.

In order to obtain a steady particle concentration, i.e. independent from the injected number of particles, simulations have been repeated by varying the number of samples. It has been observed that a stable, constant particle concentration has been obtained with 10^5 trajectories.

As shown in Fig. 2, two main OT layouts have been considered, i.e. with external (A1) and internal (A2) contamination configuration, according to the location of the aerosol challenge generators, as specified by DIN 1946-4 [27]. The experimental measurements have been conducted for these two configurations and their results compared with the corresponding CFD simulations. Moreover, two additional variations of scenario A2 have been numerically simulated by varying the status of the doors (open vs closed), and the number of open return grilles. The four layout scenarios are summarized in Table 2. The protection grade SG has been determined as:

Table 4
Range of measured data (Min-Max) for cases A1 and A2. Values of particle concentration (≥0.5 μm), temperature and air velocity for different locations (Fig. 3).

Location	Particle [PP/m^3]		T [°C]		Velocity [m/s]	
	Min	Max	Min	Max	Min	Max
P1	0	0	21.2	21.8	0.23	0.32
P2	0	0	21.2	21.7	0.22	0.3
P3	1.28 E + 03	1.90 E + 03	21.1	21.4	0.21	0.29
M1	0	0	21.9	22.1	0.32	0.41
M2	0	0	21.8	22	0.36	0.43
M3	0	0	21.4	21.7	0.34	0.44
S1	1.28 E + 07	9.73 E + 06	–	–	–	–
S2	4.37 E + 06	4.97 E + 06	–	–	–	–
EXB1	9.17 E + 06	1.36 E + 07	22.1	22.5	1.05	1.28
EXT1	9.19 E + 06	9.78 E + 06	22.2	22.3	1.37	1.55
EXB2	1.70 E + 07	1.74 E + 07	22.4	22.8	1.11	1.43
EXT2	1.92 E + 07	2.20 E + 07	22.3	22.6	1.45	1.55
EXB3	2.86 E + 07	3.46 E + 07	22.2	22.4	0.97	1.32
EXT3	3.63 E + 07	3.92 E + 07	22.3	22.4	1.36	1.66
EXB4	8.43 E + 06	9.85 E + 06	22.1	22.4	1.06	1.22
EXT4	3.41 E + 06	3.81 E + 06	22.2	22.3	1.27	1.8

$$SG_x = -\log\left(\frac{C_x}{C_{Ref}}\right) \tag{10}$$

where C_x is the mean particle concentration at measuring point x, in PP/m^3, and C_{Ref} is the reference particle concentration, in PP/m^3.

4. Experimental setting

The experimental tests have been carried out for two scenarios, namely A1 and A2 from Table 2, and shown in Fig. 2a) and b) respectively. The specifications prescribed by the DIN 1946-4 [29] in terms of geometry, heat fluxes, contamination challenge load and measuring points have been fulfilled. The dummies were made of nonwoven synthetic antistatic material (mod. Sprayguard, Indutex SpA), with 99,9% filtration efficiency for particle ≥0.5 μm which should limit particles and fibers release. Dummies have been inflated by a small fan. The challenge contamination, e.g. the artificial contamination used during tests, has been generated by a liquid nebulizer with a binary nozzle (mod. UGF 2000, Palas GmBH), which maintains a constant flow of DEHS (Di-Ethyl-Hexyl-Sebacat) airborne particles. The generated aerosol has then been conveyed to a six-way aerosol distributor and homogeneously distributed to six aerosol diffusers located close to the operating table (see Fig. 2). An optical particle counter (OPC, mod. Solair 3100+, Lighthouse), equipped with a dilution system, has monitored the particle concentration released in the OT by the six aerosol diffusers. The OPC counting efficiency was 49.2% for particle diameters of 0.3 μm and 98.1% for particle diameters greater than 0.45 μm, coincidence loss was 5% with a concentration limit of 5×10^5 PP/ft^3 according to ISO 21501-4 [35]. Two dilution systems in sequence (mod. DIL 551 and DIL 550, Topas GmBH) have diluted by a factor thousand the particle concentration sampled from the aerosol distributor and have then conveyed it to the OPC inlet. The flow rate of the OPC and of the air dilution system was 1 ft^3/min. The reference particle concentration (C_{Ref}) value for the OT has been set at 44.2×10^6 PP/m^3 for particle diameters greater than 0.5 μm instead of 35.3×10^6 PP/m^3 prescribed by the DIN 1946-4 [27]. This higher value has been chosen in order to test the OT in worst case conditions. The airborne particle concentration within the OT has been measured with the same OPC previously described. The velocity at the ceiling filter and at the extraction grilles has been measured with a rotating vane anemometer (mod. 5725, TSI Inc.; uncertainty ±1% of reading ±0.02 m/s) positioned 0.15 m far away from the filter surface or grilles. The temperature and the velocity elsewhere in the OT have been monitored with a thermo-anemometer probe (mod. 964, TSI Inc.; uncertainty ±0.015 m/s for velocity, ± 0.3 °C for temperature). The sampling time for each measurement has been set equal to 5 minutes. Fig. 3 shows the locations and the type of measurements taken during the experimental campaign.

5. Results and discussions

Experimental tests have been carried out under two scenarios for the operating room, i.e. external (A1) and internal (A2) contamination, according to DIN 1946-4 [27]. The experimental results have been used for the comparison and validation of the numerical simulations, considered as reference cases. The

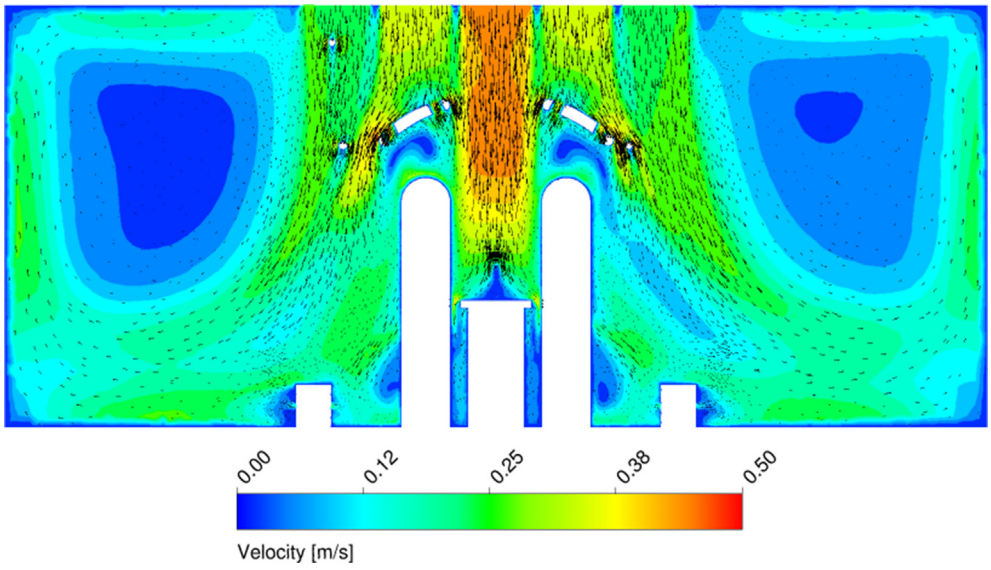

Fig. 5. Velocity vectors on the plane T for the case A1 (see Fig. 3 for plane location).

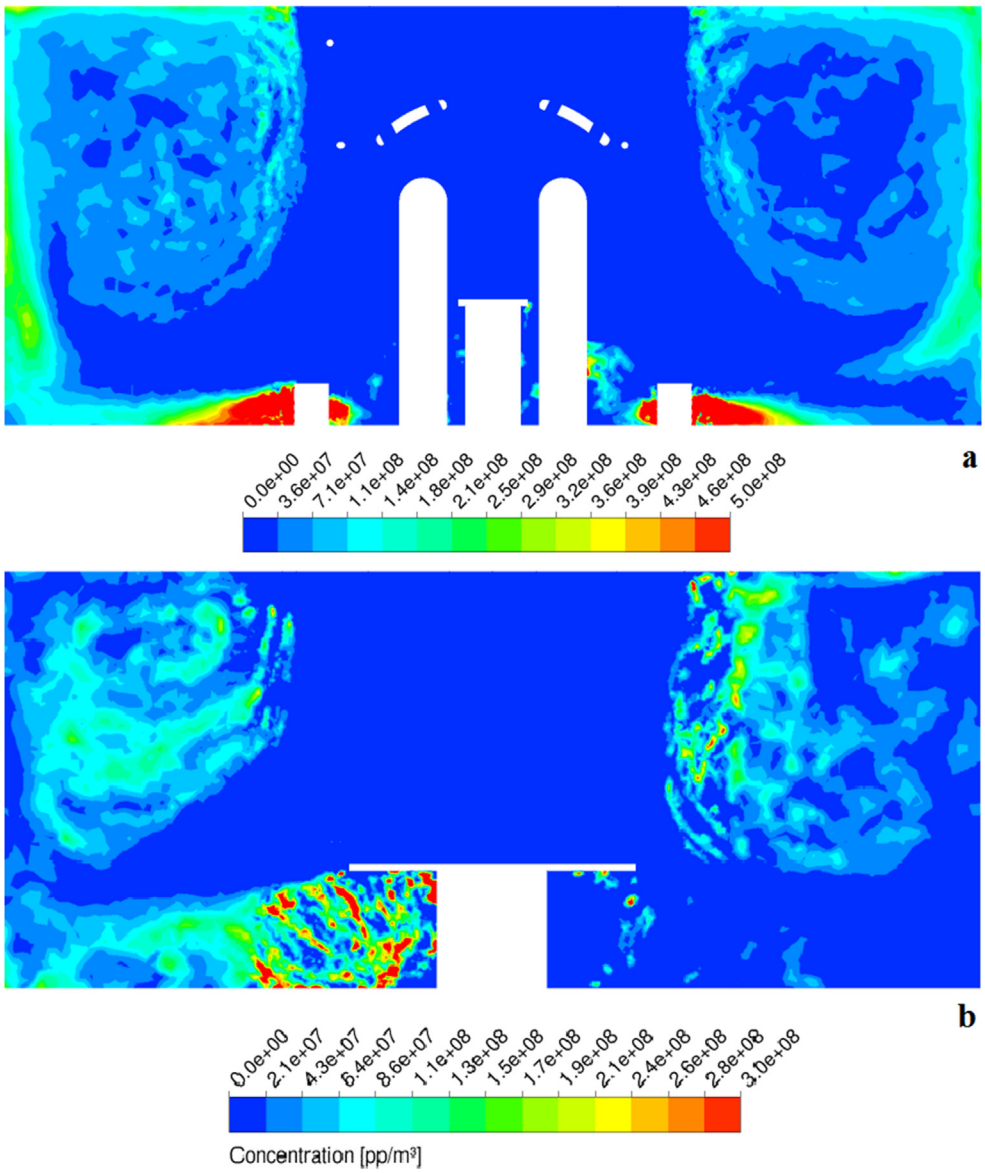

Fig. 6. Concentration contours on the plane T (a) and the plane S (b) for case A1 (see Fig. 3 for plane location).

assumptions made regarding the applicability of the DPM approach have been fully respected, i.e. the volume fraction of the dispersed phase was less than 1% as well as Eq. (7) was satisfied.

In both scenarios A1 and A2, the experimental particle concentrations over the operating table at three different positions (P1:Head, P2:Thorax and P3:Feet), see Fig. 3, were similar to those evaluated with the numerical simulations. No particles have been found at locations P1 and P3. Therefore the best achievable protection grade, SG = 5, has been obtained both experimentally and numerically, as shown in Table 3.

The differential airflow diffusion system has proven to be efficient in avoiding the presence of the airborne particles on the surgical (operating) table, thus reducing the risk for the patient of surgical site infections (SSI). On the thorax area (P2) a non-zero particle concentration has been measured in both scenarios A1 and A2. However, its value was largely below the threshold, fixed at 3520 pp/m^3 for particles larger or equal than 0.5 μm, necessary to achieve a class ISO 5. Therefore, the SG value was quite close to the simulated one (4.4 vs 5) for both scenarios. The pressurized air dummies, located close to the operating table, have been identified to be the reason for the discrepancy between the experimental and the simulated concentrations because of their particle release in the proximity of the central part of the OT table. This particle release has been most reasonably caused by an imperfect or damaged sealing of the fabric. According to standard ISO 14644-1 [12], the ISO class on the surgical table was equal to 4.8 for both scenarios A1 and A2. Fig. 4 shows the comparison between experimental and numerical results, based on the average values of the two scenarios tested, and Table 4 shows the range of measured data. The measuring points locations are shown in Fig. 3. The experimental and numerical data for temperature (Fig. 4a) and velocity (Fig. 4b) are in good agreement. The value of the mean absolute percentage error (MAPE) is less than 2% for temperature, 10% for velocity and 42% for particle concentration. The position of the extraction grilles at the four OT corners, and the airflow rate partition between top and bottom grilles (see Table 1) led to a uniform airborne particle concentration at each corner of the OT (see Fig.4c). However, large differences in particle concentrations were present between the

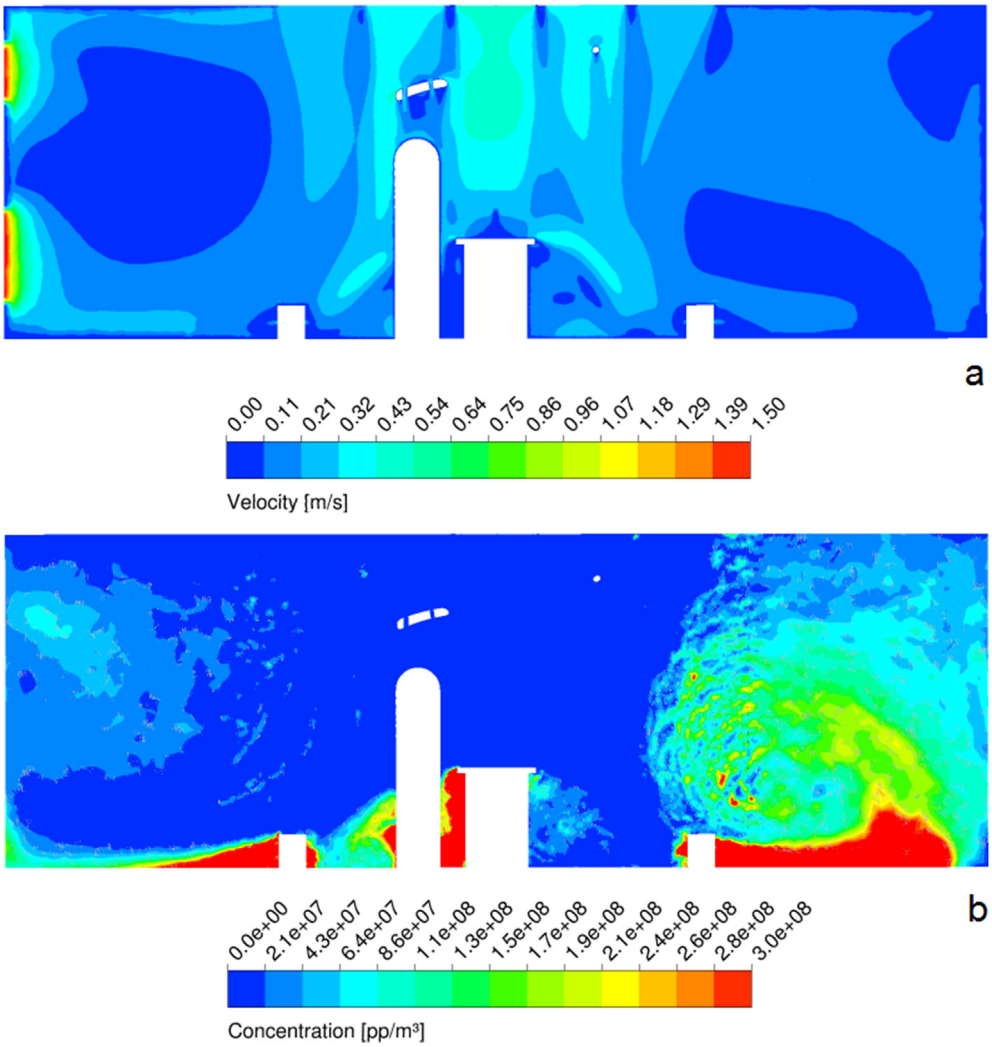

Fig. 7. Velocity (a) and Concentration contours (b) on the diagonal plane D for the case B2 (see Fig. 3 for plane location).

four extraction grilles. Those close to the main door (EX2 and EX3) presented higher particles concentrations than the others (EX1 and EX4) because of the extra dummy and medical equipment (see Fig. 2) on this side. The differential velocity of the ceiling diffuser influenced the airflow path behavior around the surgical lamp, the operating table and outside the critical zone. As shown in Fig. 5, the three HS filters generated an undisturbed unidirectional airflow over the operating table while the airflow released by the six MS filters was partially deviated by the two surgical lamps. However, the latter airflow slightly influenced the one generated by the HS filters.

The differential air velocities imposed by the ceiling filters, with decreasing intensity from the center to the periphery, allowed the air released by the HS filters to follow a preferential escape path towards the external OT area, without being influenced by the airflow released by the outer filters (MS, LS) at lower velocities. This ensured a proper flushing of the operating area close to the surgical table by entraining the particles in the high speed air stream, which was then deviated to the areas where the extraction grilles were located.

As shown in Fig. 5, there are large areas of stagnating low-speed air close to the perimeter walls of the OT, where no extraction grilles are installed. As shown in Fig. 6, compared to the central part of the OT, a higher concentration of contaminant was here simulated and also detected during the experimental tests, as shown in Fig. 4c.

Because of the good agreement between experimental and numerical results obtained with the test case scenarios A1 and A2, further simulations, by varying some layouts characteristics, have been performed, instead of time consuming and costly experimental tests. Indeed, scenario B2 has been aimed to investigate how the airflow pattern and the air contamination could be affected by the extraction grilles EX1 (Fig. 2) completely closed. The critical area under the ceiling filter has not been influenced by such a change in terms of cleanliness level, of protection class SG and airflow parameters. On the contrary, as shown in Fig. 7a and b, a wide region of slow recirculating air at high particle concentration can be detected close to the occluded extraction grilles. This high and localized airborne particle concentration may be eventually harmful, in case of particle entrainment, for the surgical personnel. The scenario C2 has investigated the effect of keeping the main door opened during a normal operation on the airflow pattern and on the particle concentration. Fig. 8 clearly shows a preferential airflow path direction which modifies normal conditions within the OT environment. Indeed, not only the particles concentration increases by approaching the exit way but also the area opposite to the main door is influenced.

Nevertheless, cleanliness condition and protection grade SG under the ceiling filter canopy and over the OT table have not been

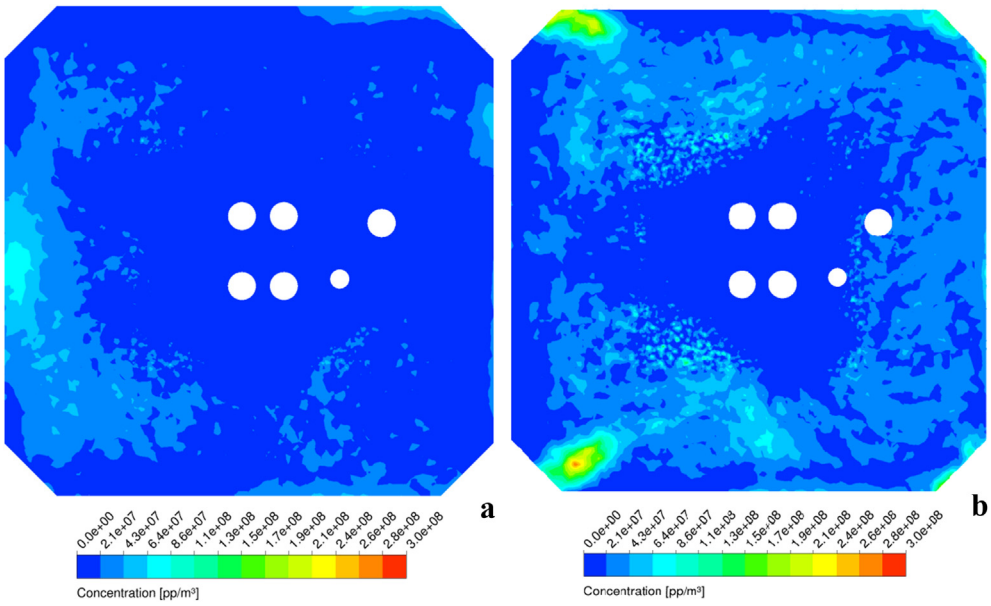

Fig. 8. Concentration contours on the plane R along Z axis for the case A2 (a) and C2 (b), (see Fig. 3 for plane location).

modified, with the sole exception of the portion of surgical table close to the main door, which is slightly affected by the suction effect created by the depression caused by the door opening (see Fig. 9), anyway maintaining an SG Grade equal to 5. Therefore, also in off-design conditions the differential air diffusion system has proven to be efficient in reducing the concentration of airborne particles over the surgical table, thus reducing the risk of possible SSI infections.

6. Conclusions

The work carried out in this study has proven how CFD modeling is an important tool to simulate the real performance of an OT in terms of airborne particle contamination control. An OT with a layout according to the German Standard DIN 1946-4 has been experimentally and numerically investigated. In particular, the effectiveness of a differential airflow diffusion system on reducing the concentration of airborne particles above the operating table has been analyzed. The numerical and the experimental results have shown a good agreement, except for a small difference in the protection grade SG, while an ISO cleanliness class 5 has been amply respected. Furthermore, two off-design scenarios have been simulated, in order to verify the influence on the airflow and concentration distribution of some occluded extraction grilles, position of the dummies and the main door opened. Nevertheless, the ceiling diffuser with differential air velocity evaluated in this work has proven to be efficient in reducing the level of airborne particle contamination over the surgical table in all evaluated configurations, even in off-design conditions, thus reducing the risk of possible SSI for patients. However, future development must be done in order to evaluate the influence of particle source challenge in positions different from the one imposed by standards and preferably with movable bodies, like humanoids, in order to more closely simulate real OT scenarios even in transient conditions.

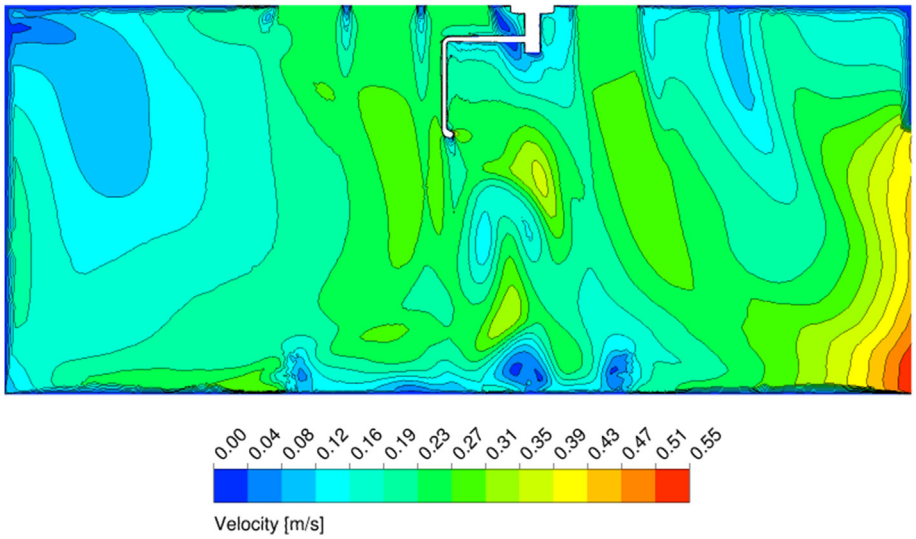

Fig. 9. Velocity contours on the plane Q for the case C2, (see Fig. 3 for plane location).

Acknowledgments

Authors want to thank Chiara Di Santis and Christian Rossi for their help. Thanks also to SagiCofim SpA and San Gerardo Hospital in Monza for the possibility to use the OT for the experimental tests.

References

[1] Chow TT, Yang XY. Performance of ventilation system in a non-standard operating room. Build Environ 2003;38:1401–11.
[2] Sadrizadeh S, Holmberg S. Surgical clothing systems in laminar airflow operating room: a numerical assessment. J Infec Public Health 2014;7:508–16.
[3] Sadrizadeh S, Tammelin A, Ekolind P, Holmberg S. Influence of staff number and internal constellation on surgical site infection in an operating room. Particuology 2014;12:42–51.
[4] Chow TT, Wang J. Dynamic simulation on impact of surgeon bending movement on bacteria-carrying particles distribution in operating theatre. Build Environ 2014;57:68–80.
[5] Rui Z, Guangbei T, Jihong L. Study on biological contaminant control strategies under different ventilation models in hospital operating room. Build Environ 2008;43:793–803.
[6] Chow TT, Yang XY. Ventilation performance in the operating theatre against airborne infection: numerical study on an ultra-clean system. J Hosp Infect 2005;59:138–47.
[7] Dascalakia EG, Lagoudib A, Balarasa CA, Gaglia AG. Air quality in hospital operating rooms. Build Environ 2008;43:1945–52.
[8] Stacey A, Humphreys H. A UK historical perspective in operating theatre ventilation. J Hosp Infect 2002;52:77–80.
[9] Charnley J, Eftekhar N. Postoperative infection in total prosthetic replacement arthroplasty of the hip-joint. With special reference to the bacterial content of the operating room. Br J Surg 1969;56:641–9.
[10] Whyte W, Hodgson R, Tinkler J. The importance of airborne bacterial contamination of wounds. J Hosp Infect 1982;3:123–35.
[11] Lidwell OM, Lowbury EJL, White W, Blowers R, Stanley SJ, Lowe D. Airborne contamination of wounds in joint replacement operations: the relationship to sepsis rates. J Hosp Infect 1983;4:111–31.
[12] ISO 14644-1. Cleanrooms and associated controlled environments- Part 1: classification of air cleanliness. Geneva, Switzerland: International Organization for Standardization; 1999.
[13] ISO 14698:1–2. Cleanrooms and associated controlled environments – Biocontamination control. Geneva, Switzerland: International Organization for Standardization; 2003.
[14] Sun Z, Wang S. A CFD-based test method for control of indoor environment and space ventilation. Build Environ 2010;45:1441–7.
[15] Swift J, Avis E, Millard B, Lawrence TM. Air distribution strategy impact on operating room infection control. In: Proceedings of clima-wellbeing indoors; 2007 [Helsinki, Finland].
[16] Memarzadeh F, Manning A. Comparison of operating room ventilation systems in the protection of the surgical site. ASHRAE Trans 2002;108(2):3–15.
[17] Memarzadeh F, Jiang Z. Effect of operation room geometry and ventilation system parameter variations on the Protection of the surgical site. In: Proceedings of IAQ; 2004 [Tampa, USA].
[18] Kameel R, Khalil EE. Simulation of flow, heat transfer and relative hu-midity characteristics in air-conditioned surgical operating theaters. In: Proceedings of 41st aerospace sciences meeting and exhibit; 2003 [Reno, Nevava, USA].
[19] Brohus H, Hyldig ML, Kamper S, Vachek UM. Influence of disturbances on bacteria level in an operating room. Proceedings of Indoor Air. In: The 11th international conference on indoor air quality and climate, Copenhagen, Denmark; 2008.
[20] Shuyun D, Guangbei T, Rongguang C, Zhenfeng Y. Numerical study on effects of door-opening on air flow patterns and dynamic cross contamination in an ISO class 5 operating room, 15. Tianjin, China: Transactions of Tianjin Uni-versity; 2009. p. 210–5.
[21] Tung YC, Shih YC, Hu SC. Numerical study on the dispersion of airborne contaminants from an isolation room in the case of door opening. Appl Therm Eng 2009;29:1544–51.
[22] Srebric J, Vukovic V, He G, Yang X. CFD boundary conditions for contaminant dispersion, heat transfer and air flow simulations around human occupants in indoor environments. Build Environ 2008;43(3):294–303.
[23] SIS-TS 39. Microbiological cleanliness in the operating room - preventing airborne contamination - guidance and fundamental requirements. SIS. Stockholm, Sweden: Swedish Standard Institute; 2012.
[24] NF S90-351. Établissements de santé - Zones à environnement maîtrisé - Exigences relatives à la maîtrise de la contamination aéroportée. Paris, France: ANFOR, Association Francaise de Normalisation; 2013.
[25] Standard 170-2013. Ventilation of health care facilities. Tullie Circle, Atlanta, USA: ANSI/ASHRAE/ASHE; 2013.
[26] SWKI 99-3E. Heating, ventilation and air-conditioning system in hospitals. Schonbuhl, CH: Schweizerischer Verein von Warme- und Klimaingenieuren Sekretariat; 2004.
[27] DIN 1946-4. Ventilation and air conditioning, Part 4: Ventilation in buildings and rooms of health care. Berlin, DE: Deutsches Institut für Normung; 2008.
[28] Traversari AAL, Goedhart CA, Dusseldorp E, Bode A, Keuning F, Pelk MSJ, et al. Laying-up of sterile instruments in the operating theatre: equal or superior protection by using a horizontal unidirectional air flow system. J Hosp Infect 2013;85:125–33.
[29] Zhang Z, Chen Q. Comparison of the Eulerian and Lagrangian methods for predicting particle transport in enclosed spaces. Atmos Environ 2007;41(25):5236–48.
[30] Shih TH, Liou WW, Shabbir A, Zhu J. A new k- epsilon Eddy-viscosity model for high Reynolds number turbulent flows - model development and validation. Comput Fluids 1995;24:227–38.
[31] Morsi SA, Alexander AJ. An investigation of particle trajectories in two-phase flow systems. J Fluid Mech 1972;55:193–208.
[32] Ansys Inc. Fluent theory guide v.15. 2014.
[33] Crowe CT, Sommerfeld M, Tsuji T. Multiphase flow with droplet and particles. Boca Roton: CRC Press; 1998.
[34] Marocco L, Mora A. CFD modeling of the dry-sorbent-Injection process for fuel gas desulfurization. Sep Purif Technol 2013;108:205–14.
[35] ISO 21501. Determination of particle size distribution - single particle light interaction methods - part 4: light scattering airborne particle counter for clean spaces. Geneva, Switzerland: International Organization for Standardization; 2007.